Density Reduction and Mechanical Performance of Metakaolin-Based Alkali-Activated Composites Containing EPS Beads

Adriano Galvão Souza Azevedo*

Department of Biosystems Engineering, Research Center on Materials for Biosystems (BioSMat), University of São Paulo (USP), Brazil

Abstract: Lightweight alkali-activated composites offer a route to reducing component mass while retaining useful mechanical performance. This study examines how the volume fraction and particle size of expanded polystyrene (EPS) control the physical, microstructural, and mechanical behavior of metakaolin-based alkali-activated composites. A full 3^2 factorial design was adopted using EPS contents of 18, 35, and 53 vol.% and average bead diameters of 0.85, 2.16, and 6.00 mm. The metakaolin was activated with an 8 M NaOH solution combined with sodium silicate, and the composites were evaluated after 28 days by X-ray diffraction, infrared spectroscopy, scanning electron microscopy, water absorption, apparent porosity, density, and compressive strength. The alkali-activation reaction produced an aluminosilicate binder without detectable interference from EPS incorporation. Increasing the EPS content progressively reduced density, with the largest reduction obtained for the coarsest beads. Composites containing 53 vol.% EPS reached densities as low as 0.80 g cm^{-3}. This reduction was accompanied by a decrease in compressive strength, from approximately 47.5 MPa for the reference matrix to 14 MPa for composites containing 53 vol.% of 0.85 mm EPS and to 1.5 MPa when the same volume fraction of 6.00 mm beads was used. SEM observations associated the greater strength loss of coarse-EPS composites with wider interfacial discontinuities and crack formation around the polymeric inclusions. Despite this trade-off, selected formulations combined densities of 0.8–1.2 g cm^{-3} with compressive strengths of 15–25 MPa, indicating potential for lightweight non-structural building components.

Keywords: Alkali-activated composite, Metakaolin, Expanded polystyrene, Lightweight material, Density–strength relationship.

1. INTRODUCTION

Reducing the self-weight of construction components can lower handling demands, decrease permanent structural loads, and expand the range of prefabricated and insulating products. At the same time, the environmental burden associated with ordinary Portland cement production has intensified the search for alternative binders with lower clinker demand and competitive engineering performance [1, 2]. Alkali-activated materials (AAMs), produced by reacting aluminosilicate precursors with alkaline solutions, are among the most widely investigated alternatives. Depending on precursor chemistry, activator composition, and curing conditions, these binders can develop high early strength, thermal stability, and resistance to aggressive environments [3-9].

The structure of alkali-activated aluminosilicate binders is commonly described in terms of interconnected Si–O–Al units whose arrangement depends strongly on the Si/Al ratio (Table **1**) [10-14]. During activation, the reactive fraction of the precursor dissolves in the alkaline medium, releasing silicate and aluminate species that subsequently reorganize and condense into a three-dimensional binding network. This chemistry provides considerable flexibility for incorporating dispersed phases and tailoring density, transport properties, and mechanical response.

Table 1: Representative Aluminosilicate Structural Units Associated with Alkali-Activated Binders

Monomer	Si/Al ratio
Poly(sialate) (-Si-O-Al-O-)	1:1
Poly(sialate-siloxy) (-Si-O-Al-O-Si-O-)	2:1
Poly(sialate-disiloxy) (-Si-O-Al-O-Si-O-Si-O-)	3:1

Although alkali-activated binders have been studied for several decades [15-17], the development of lightweight formulations remains challenging because density reduction is generally accompanied by loss of stiffness and compressive strength. One practical strategy is the replacement of part of the dense mineral matrix by low-density inclusions. The resulting performance depends not only on the amount of lightweight phase, but also on its dimensions, spatial distribution, and adhesion to the surrounding binder [18-22].

Expanded polystyrene is a closed-cell polymeric material formed by expanding polystyrene beads with steam. The final product contains approximately 98% air and therefore presents a very low bulk density, together with thermal and acoustic insulation capacity

*Address correspondence to this author at the Department of Biosystems Engineering, Research Center on Materials for Biosystems (BioSMat), University of São Paulo (USP), Brazil;
E-mail: adrianogalvao@usp.br

Received on 03-07-2026 Accepted on 29-07-2026 Published on 03-08-2026

E-ISSN: 2410-4701/26

[23]. These characteristics have encouraged its use as a lightweight aggregate in Portland-cement concretes. However, the hydrophobic and mechanically compliant nature of EPS can produce weak interfacial regions, stress concentrations, and reductions in strength, particularly when large particles or high volume fractions are employed.

In recent years, the incorporation of EPS into alkali-activated materials has also attracted increasing attention as an effective strategy for producing lightweight composites with improved thermal insulation and reduced environmental impact. Previous studies have consistently demonstrated that increasing the EPS content leads to substantial reductions in bulk density, although these improvements are generally accompanied by losses in compressive strength due to the low stiffness of the polymeric particles and the formation of weak interfacial regions. Nevertheless, most published investigations have primarily focused on the influence of EPS content, while comparatively less attention has been devoted to understanding how particle size affects the microstructure, interfacial characteristics, and mechanical performance of alkali-activated composites [24-27].

Furthermore, relatively few studies have attempted to correlate density reduction with changes in water transport properties and microstructural features in order to explain the mechanisms governing mechanical performance. As a result, the respective contributions of matrix continuity, interfacial integrity, and EPS geometry to the density–strength relationship remain insufficiently understood, particularly in metakaolin-based alkali-activated systems.

Although several studies have investigated the incorporation of EPS into alkali-activated materials, most have primarily focused on the influence of EPS content on density reduction and mechanical performance. Comparatively fewer studies have systematically evaluated the combined effect of EPS particle size and volumetric fraction while correlating the resulting physical, mechanical, and microstructural characteristics. Consequently, the mechanisms governing the relationship between matrix continuity, interfacial characteristics, and composite performance remain insufficiently understood.

To address this knowledge gap, the present study systematically investigates the combined influence of EPS particle size and volume fraction on the physical, mechanical, and microstructural behavior of metakaolin-based alkali-activated composites. Lightweight composites containing 18, 35, and 53 vol.% EPS with average bead diameters of 0.85, 2.16, and 6.00 mm were produced and characterized in terms of density, water absorption, apparent porosity, compressive strength, X-ray diffraction, Fourier-transform infrared spectroscopy, and scanning electron microscopy. By integrating these complementary analyses, this work seeks to clarify the mechanisms governing the density–strength relationship and to identify optimized lightweight formulations capable of combining significant density reduction with satisfactory mechanical performance.

2. MATERIALS AND METHODS

2.1. Raw Materials

Commercial metakaolin supplied by Metacaulim do Brasil LTDA was used as the aluminosilicate precursor. Its chemical composition is reported in Table **2**. The alkaline activator was prepared from analytical-grade sodium hydroxide (98% purity, Sulfal Química LTDA) and commercial sodium silicate solution (Diatom®, R-2252). The composition and physical properties of the sodium silicate are given in Table **3**. Expanded polystyrene beads were used as the lightweight dispersed phase. Three grades with average diameters of 0.85, 2.16, and 6.00 mm were selected, as illustrated in Figure **1**. Their corresponding densities are listed in Table **4**.

Table 2: Chemical Composition of the Metakaolin used in the Alkali-Activated Matrix (wt.%)

SiO_2	Al_2O_3	Fe_2O_3	TiO_2	CaO	MgO	K_2O	Na_2O	SO_2	LOI
58.7	33.4	2.1	1.3	0.1	0.2	1.6	0.1	0.2	2.3

LOI = loss on ignition.

Table 3: Composition and Physical Properties of the Sodium Silicate Solution, as Supplied by the Manufacturer

Composition		Total solids	Humidity	Density (g/cm^3)	Viscosity (cP)
Na_2O	14.98%	48.5%	51.45%	1.58	1.35
SiO_2	33.57%				
SiO_2/Na_2O	2.40				

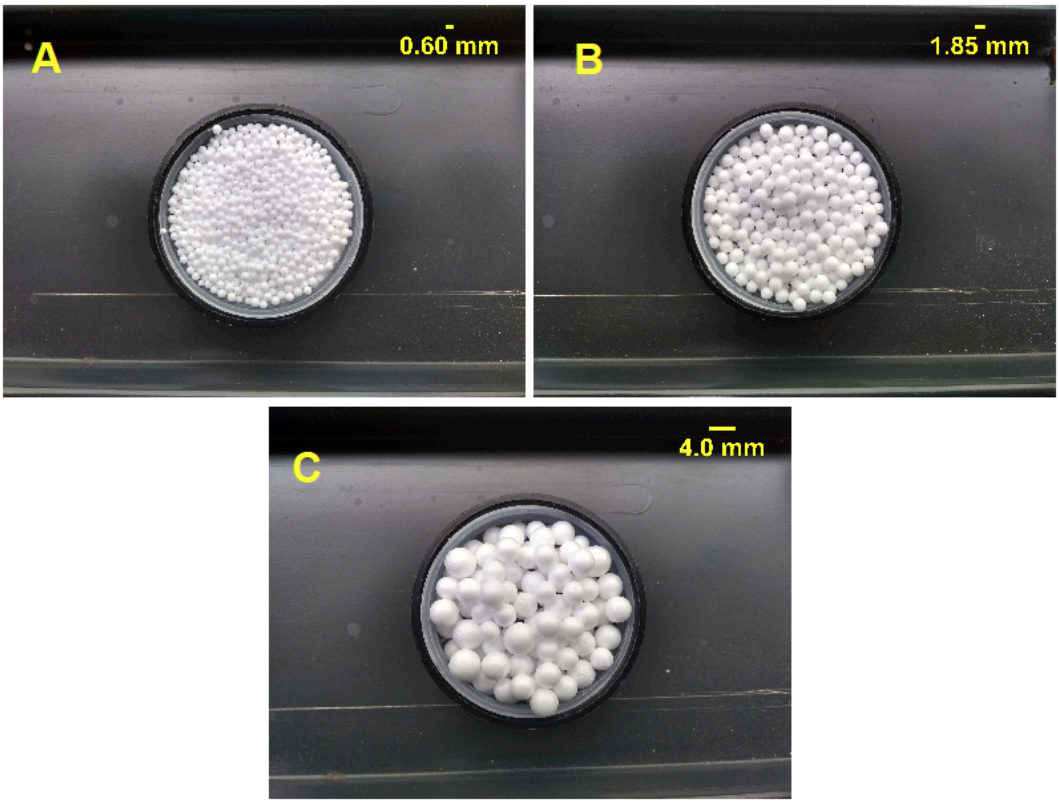

Figure 1: EPS beads with average diameters of (**A**) 0.85 mm, (**B**) 2.16 mm, and (**C**) 6.00 mm.

Table 4: Average Diameter and Density of the EPS Beads used as the Lightweight Dispersed Phase

EPS Sample	The average diameter of EPS beads(mm)	Density EPS beads (g/cm³)
A	0.85	2.7×10^{-2}
B	2.16	1.49×10^{-2}
C	6.00	1.29×10^{-2}

2.2. Experimental Procedures

2.2.1. Preparation of the Alkaline Activator

An 8 M NaOH solution was prepared by dissolving sodium hydroxide in deionized water. The solution was stored for 24 h before use to allow the heat generated during dissolution to dissipate. Immediately before mixing, 50 wt.% of the NaOH solution was replaced by sodium silicate solution, yielding a Na_2SiO_3/NaOH solution mass ratio of 1.0.

2.2.2. Composite Preparation and Experimental Design

The alkali-activated paste was produced at room temperature using a metakaolin-to-activator mass ratio of 0.9. Additional water corresponding to 5 wt.% of the metakaolin mass was incorporated to provide adequate workability. EPS beads were then added at volume fractions of 18, 35, or 53% and manually blended until visually uniform. The mixtures were placed in cylindrical plastic molds measuring 30 mm in diameter and 60 mm in height. Each mold was filled in three layers, with approximately 20 s of vibration after placement of each layer to reduce entrapped air. The specimens were sealed with plastic film for the first 24 h, subsequently cured at 60 °C for 24 h, and then stored at room temperature (25 ± 2 °C) until testing at 28 days.

The experimental program followed the principles of factorial design and statistical analysis described by Montgomery [13] and Werkema and Aguiar [14]. Two independent factors were investigated: EPS volume fraction and average EPS particle diameter.

Both factors were evaluated at three levels. EPS contents of 18, 35, and 53 vol.% were combined with average bead diameters of 0.85, 2.16, and 6.00 mm. All other parameters were kept constant, including the metakaolin-to-activator mass ratio (0.9), Na_2SiO_3/NaOH solution mass ratio (1.0), NaOH concentration (8 M), additional water content (5 wt.% relative to metakaolin), initial thermal curing condition (60 °C for 24 h), and total curing age (28 days).

A complete 3^2 factorial design generated nine composite formulations, designated C1–C9, as summarized in Table **5**. A reference alkali-activated matrix without EPS was also prepared under the same mixing and curing conditions.

Table 5: Formulations used in the 3² Factorial Experimental Design

Formulation	MK (% vol.)	EPS (% vol.)	Average EPS diameter (mm)	MK / ($NaOH$ + Na_2SiO_3) ratio	Additional water (%)
18A	82	18	0.85	0.9	5
35A	65	35	0.85	0.9	5
53A	47	53	0.85	0.9	5
18B	82	18	2.16	0.9	5
35B	65	35	2.16	0.9	5
53B	47	53	2.16	0.9	5
18C	82	18	6.00	0.9	5
35C	65	35	6.00	0.9	5
53C	47	53	6.00	0.9	5
Ref	100	--	--	0.9	5

2.2.3. Characterization Methods

Compressive strength was determined using five specimens per formulation in accordance with NBR 5739 [28]. Tests were performed in uniaxial compression using a Shimadzu AG-X Plus universal testing machine at a crosshead speed of 2 mm min^{-1}. The load–displacement data were processed using Trapezium X software, version 1.2.6.

The microstructure and matrix–EPS interfaces were examined by scanning electron microscopy using a Hitachi TM3000 microscope equipped with a Bruker X-Flash energy-dispersive spectroscopy detector. Water absorption and apparent porosity were measured according to BS EN ISO 10545-3 [29]. Infrared spectra were collected with a PerkinElmer Spectrum 1000 spectrometer using KBr pellets prepared at a sample-to-KBr mass ratio of 1:300. Measurements covered 400–4000 cm^{-1} at a resolution of 4 cm^{-1}. Crystalline phases were analyzed by X-ray diffraction using a Shimadzu XRD-6000 diffractometer with Cu Kα radiation over a 2θ range of 5–80°. Phase identification was performed by comparison with the JCPDS database.

3. RESULTS AND DISCUSSION

3.1. Formation of the Alkali-Activated Matrix

Figure **2** compares the X-ray diffraction patterns of the metakaolin and the reference alkali-activated matrix after 28 days. The precursor contains reflections assigned to quartz (SiO_2), kaolinite ($Al_2Si_2O_5(OH)_4$), and muscovite ($KAl_2Si_3AlO_{10}(OH,F)_2$), together with a broad diffuse halo between approximately 18 and 38° 2θ. This halo indicates the presence of poorly ordered aluminosilicate material, which constitutes the main reactive fraction during alkaline activation.

Quartz and part of the crystalline kaolinite and muscovite assemblage remain detectable after activation, indicating incomplete participation of these ordered phases in the reaction. The principal change is the displacement of the diffuse halo toward higher angles, approximately 22–40° 2θ. This shift is consistent with dissolution of the reactive metakaolin fraction and formation of a new disordered aluminosilicate binding phase. The retained crystalline reflections therefore represent residual precursor minerals embedded within the reaction product rather than newly formed binding phases.

3.2. Chemical Bonding Evolution

The FTIR spectra of the metakaolin and the 28-day alkali-activated matrix are presented in Figure **3**. Broad bands near 3460 and 1660 cm^{-1} correspond to O–H stretching and H–O–H bending associated with adsorbed and structurally retained water. Their higher intensity in the activated matrix reflects the greater water content of the reaction products. The principal Si–O–T band of the metakaolin, centered near 1080 cm^{-1}, shifts to approximately 1000 cm^{-1} after activation. This displacement is attributed to the reorganization of the aluminosilicate framework and the formation of Si–O–Al linkages during polycondensation [15, 16, 18]. Bands near 540 and 470 cm^{-1} are associated with Si–O–Al and Si–O–Si vibrations, whereas features around 730 and 697 cm^{-1} are related to ring structures commonly reported in zeolitic or zeolite-like aluminosilicate environments. The band at approximately 1429 cm^{-1} is assigned to carbonate species. Its presence is consistent with carbonation of residual alkaline species and possible formation of sodium carbonate or hydrated sodium carbonate phases [22], according to Equation 1.

$$2\,NaOH + CO_2 \rightarrow Na_2CO_3 + H_2O \quad (1)$$

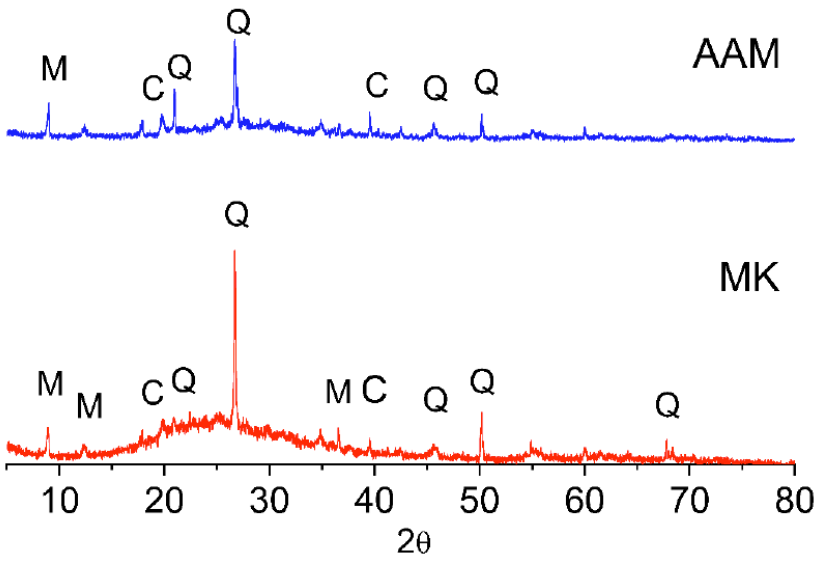

Figure 2: X-ray diffraction patterns of metakaolin and the alkali-activated matrix after 28 days. Q: quartz; M: muscovite; C: kaolinite.

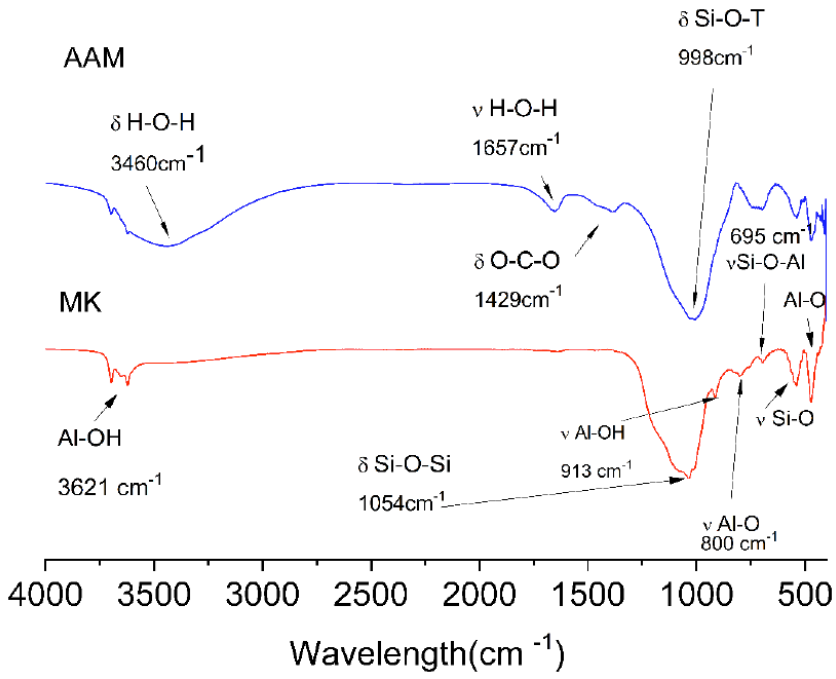

Figure 3: FTIR spectra of metakaolin and the alkali-activated matrix after 28 days.

3.3. Density and Water-Related Properties

Figure **4** summarizes the apparent porosity and water absorption results. The reference matrix exhibited an apparent porosity of approximately 40% and water absorption close to 30%. Replacing part of the alkali-activated matrix with EPS reduced the measured apparent porosity. For 0.85 mm beads, porosity decreased from about 37% at 18 vol.% EPS to approximately 27% at 53 vol.% EPS. A comparable trend was obtained with 2.16 mm beads, for which porosity declined from roughly 36% to 26.6% over the same range of EPS contents.

The largest porosity reduction occurred for composites containing 6.00 mm beads. Apparent porosity decreased from approximately 34.5% at 18 vol.% EPS to 22.2% at 53 vol.% EPS, corresponding to a reduction of about 35.6% relative to the lowest-EPS formulation in this particle-size series. This behavior reflects the progressive replacement of the intrinsically porous inorganic matrix by closed-cell polymeric inclusions that are not penetrated by water during the test.

Water absorption did not follow the same monotonic tendency as apparent porosity. At high EPS contents, particularly with coarse beads, absorption increased

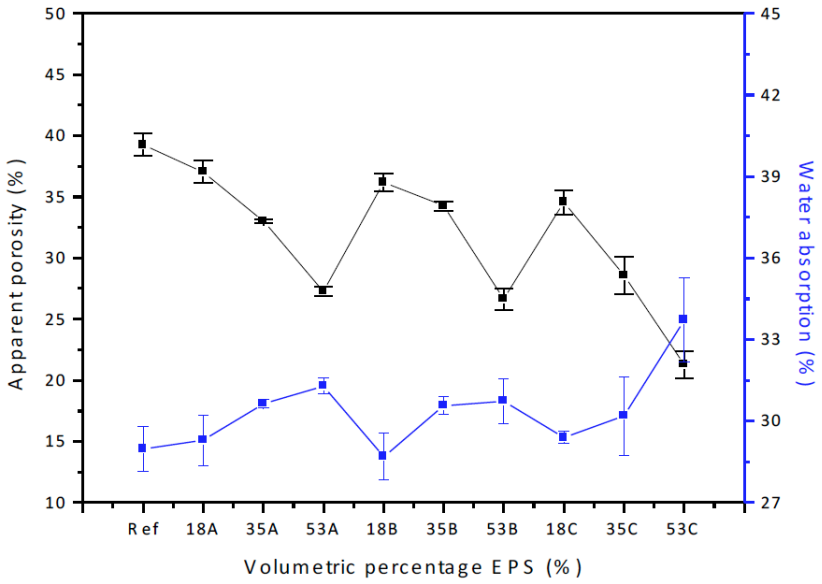

Figure 4: Apparent porosity and water absorption of the reference matrix and EPS-containing composites after 28 days.

despite the lower measured porosity. This divergence suggests that the accessible transport pathways were increasingly controlled by the matrix–EPS interfaces rather than by the volume of the polymer particles themselves. Interfacial gaps and microcracks observed by SEM can provide connected paths for water ingress even when the total quantity of water-accessible matrix is reduced.

Although the apparent porosity generally decreased with increasing EPS content, water absorption did not follow the same trend. Instead, water absorption remained relatively stable for most formulations and increased noticeably only for the composite containing the highest EPS volume fraction combined with the largest particle size (53C). This behavior suggests that water transport is governed not only by the total volume of accessible pores but also by their morphology and connectivity. At high EPS contents, especially when large particles are incorporated, localized interfacial gaps between the alkali-activated matrix and the EPS beads may become interconnected, facilitating capillary water penetration without a proportional increase in the overall apparent porosity. This interpretation is further supported by the SEM observations, which reveal more pronounced interfacial discontinuities around the larger EPS particles, providing preferential pathways for water ingress while exerting only a limited influence on the total apparent porosity.

3.3.1. Apparent Density

The apparent density results are shown in Figure **5**. The reference matrix reached approximately 2.23 g

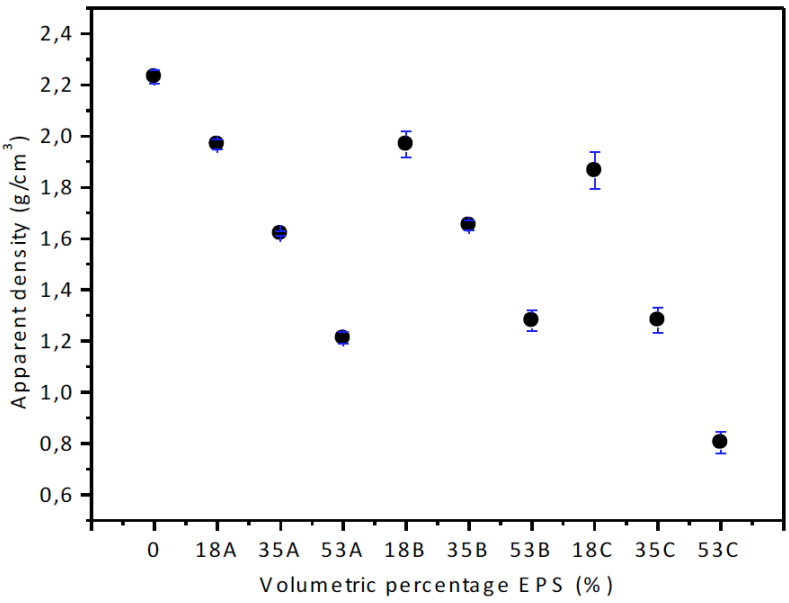

Figure 5: Apparent density of the reference matrix and EPS-containing composites after 28 days.

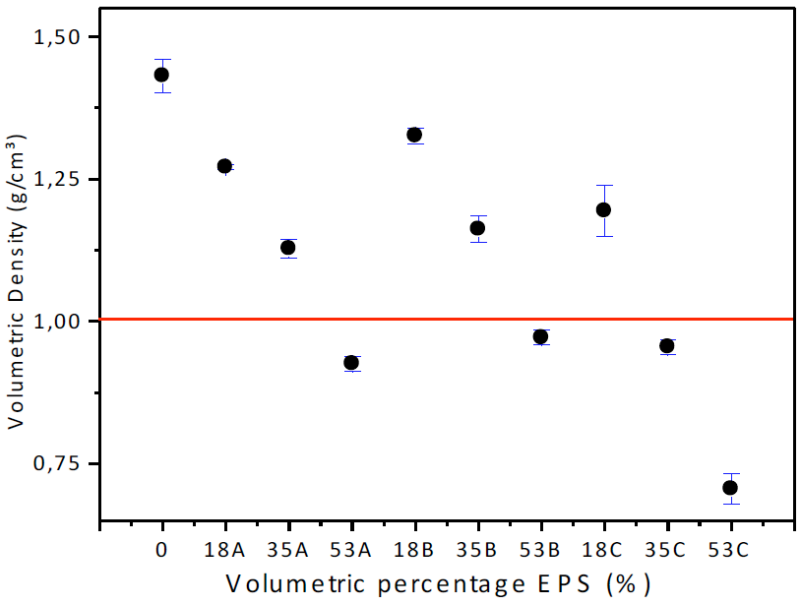

Figure 6: Volumetric density of the reference matrix and EPS-containing composites after 28 days.

cm^{-3}. EPS incorporation caused a systematic decrease because the dense aluminosilicate binder was replaced by particles with densities several orders of magnitude lower. For composites containing 0.85 mm EPS, density decreased from approximately 1.96 g cm^{-3} at 18 vol.% to 1.21 g cm^{-3} at 53 vol.%. Similar values were obtained with 2.16 mm beads, ranging from about 1.96 to 1.27 g cm^{-3}.

3.3.2. Volumetric Density

Volumetric density is a key design parameter for lightweight composites because it directly influences dead load, transport requirements, and several mechanical and thermal properties. Figure **6** confirms that density decreased as the EPS volume fraction increased. The effect was most pronounced for the 6.00 mm grade, which also had the lowest measured particle density. Formulations 18C, 35C, and 53C exhibited densities of approximately 1.86, 1.27, and 0.80 g cm^{-3}, respectively. The general tendency agrees with previous studies on EPS-containing cementitious composites [30-31]. Compositions containing 53 vol.% EPS reached densities below that of water, and the specimen containing 53 vol.% of 6.00 mm beads remained intact while floating. These results demonstrate the strong contribution of both EPS content and EPS grade to the overall density of the composite.

3.4. Microstructure and Matrix–EPS Interface

Figures **7–12** present longitudinal sections and SEM images of the reference matrix and selected composites. The reference specimen displays a relatively homogeneous and compact binder, with isolated pores and residual metakaolin particles embedded in the alkali-activated gel. The morphology confirms that the selected activator and curing procedure were sufficient to produce a continuous aluminosilicate matrix, although complete dissolution of the precursor was not achieved. In composite 18A, containing 18 vol.% of 0.85 mm EPS, the polymeric beads are generally surrounded by the binder. Local voids left by detached particles indicate that adhesion was not uniform across all interfaces. At higher magnification, however, portions of the EPS surface remain closely contacted by the matrix.

Composite 18B, produced with 2.16 mm beads at the same volume fraction, exhibits a similarly continuous matrix and EPS particles partially coated by reaction products or residual metakaolin. The morphology changes more markedly in specimens containing 6.00 mm EPS. In 18C–53C, larger interfacial discontinuities, cracks adjacent to the beads, and greater fragmentation of the cut surfaces are evident. Because EPS is hydrophobic and substantially more compliant than the surrounding inorganic binder, shrinkage and load transfer can concentrate stresses at the interface. Increasing either particle size or volume fraction enlarges the total extent and severity of these mechanically weak regions. The SEM observations therefore provide a microstructural basis for the stronger loss of compressive strength observed in composites containing coarse EPS. The SEM observations are consistent with the compressive strength results (which will be discussed later). Formulations containing smaller EPS particles exhibited a more homogeneous matrix distribution and fewer interfacial discontinuities, favoring more efficient stress transfer during loading. Conversely, the incorporation of larger EPS particles resulted in wider

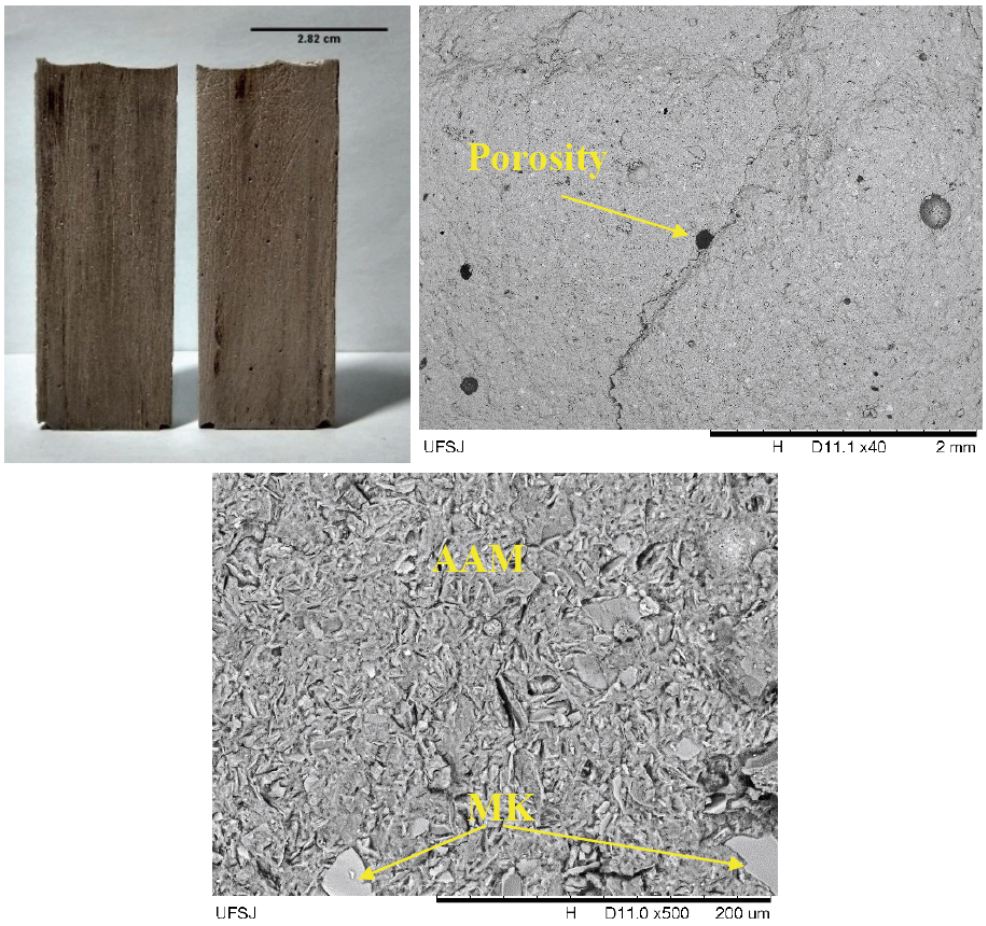

Figure 7: Longitudinal section and SEM images of the REF alkali-activated matrix after 28 days.

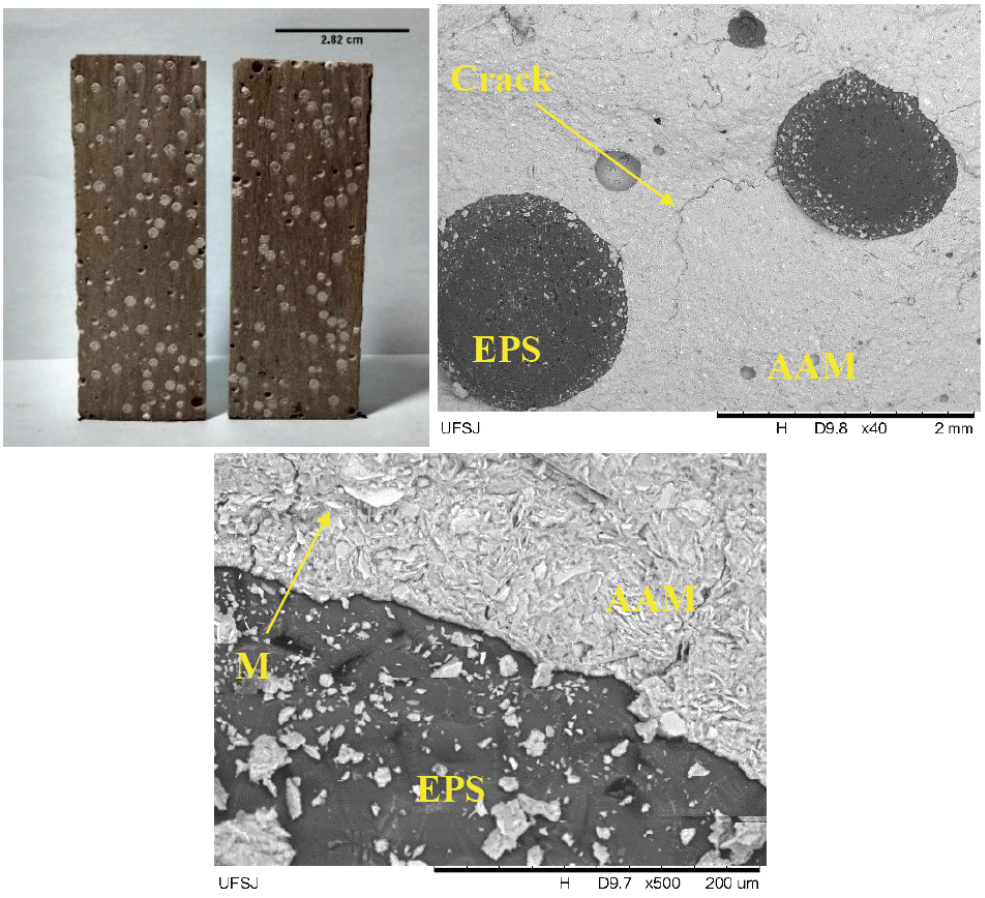

Figure 8: Longitudinal section and SEM images of composite 18A after 28 days.

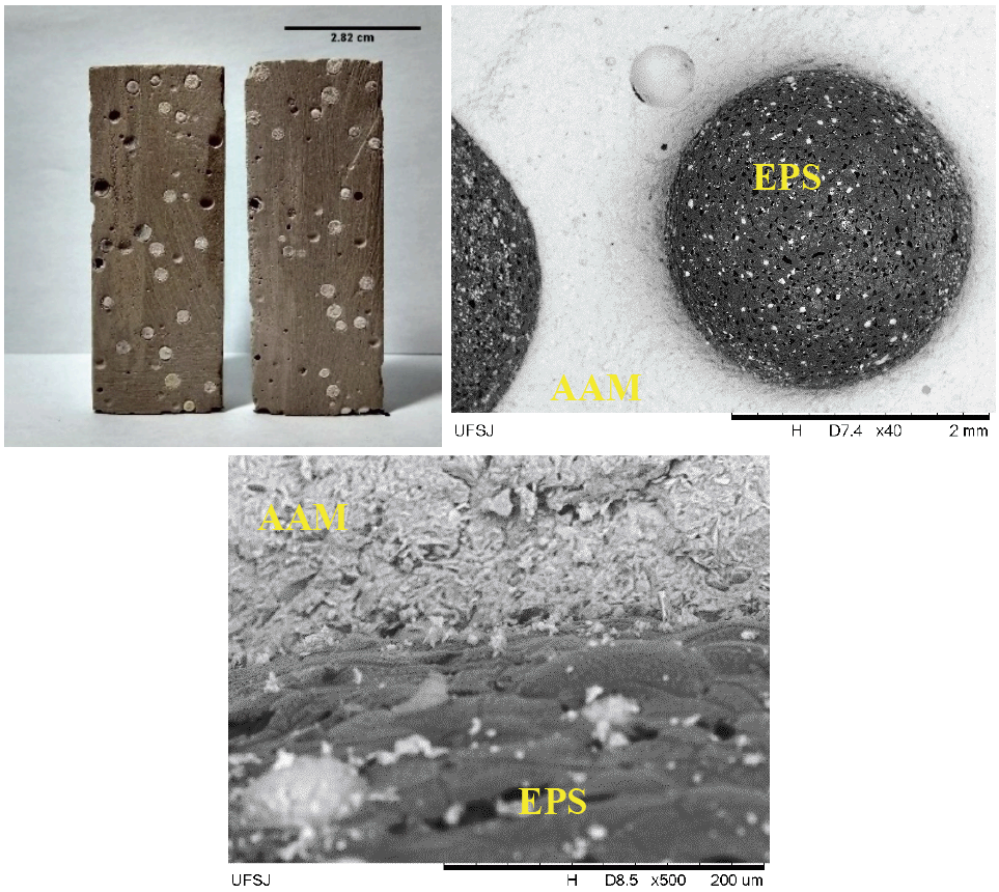

Figure 9: Longitudinal section and SEM images of composite 18B after 28 days.

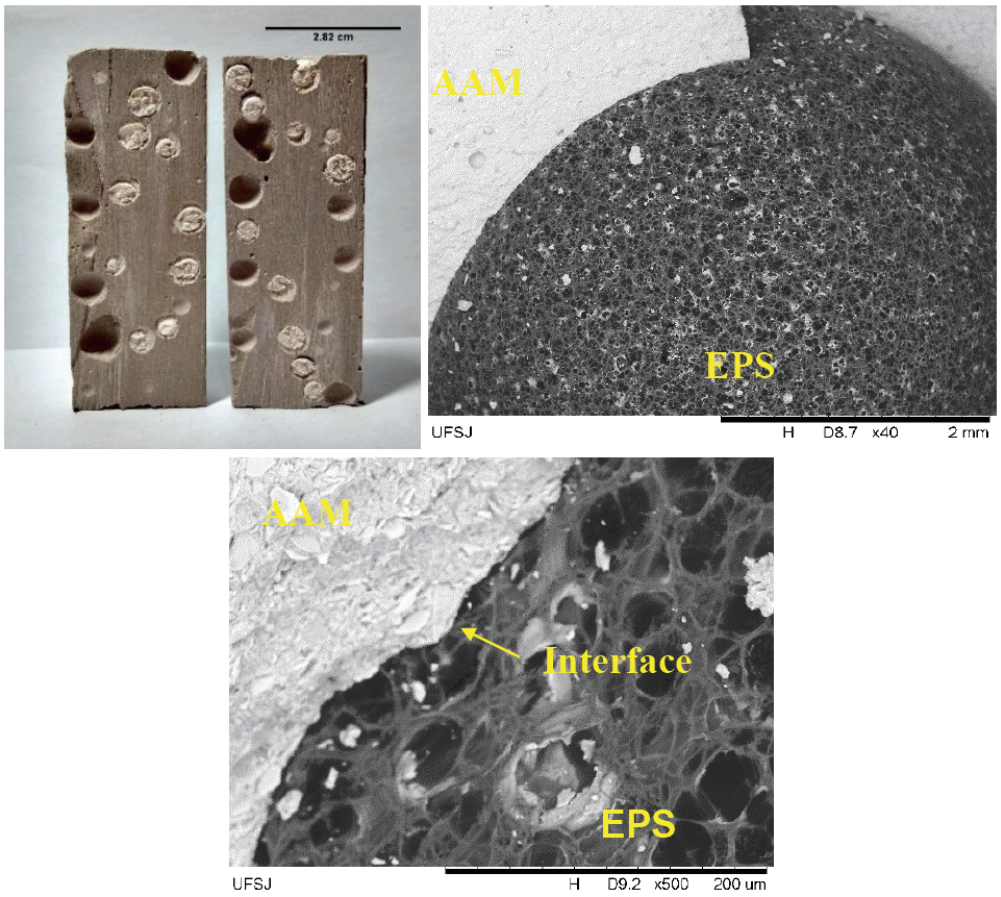

Figure 10: Longitudinal section and SEM images of composite 18C after 28 days.

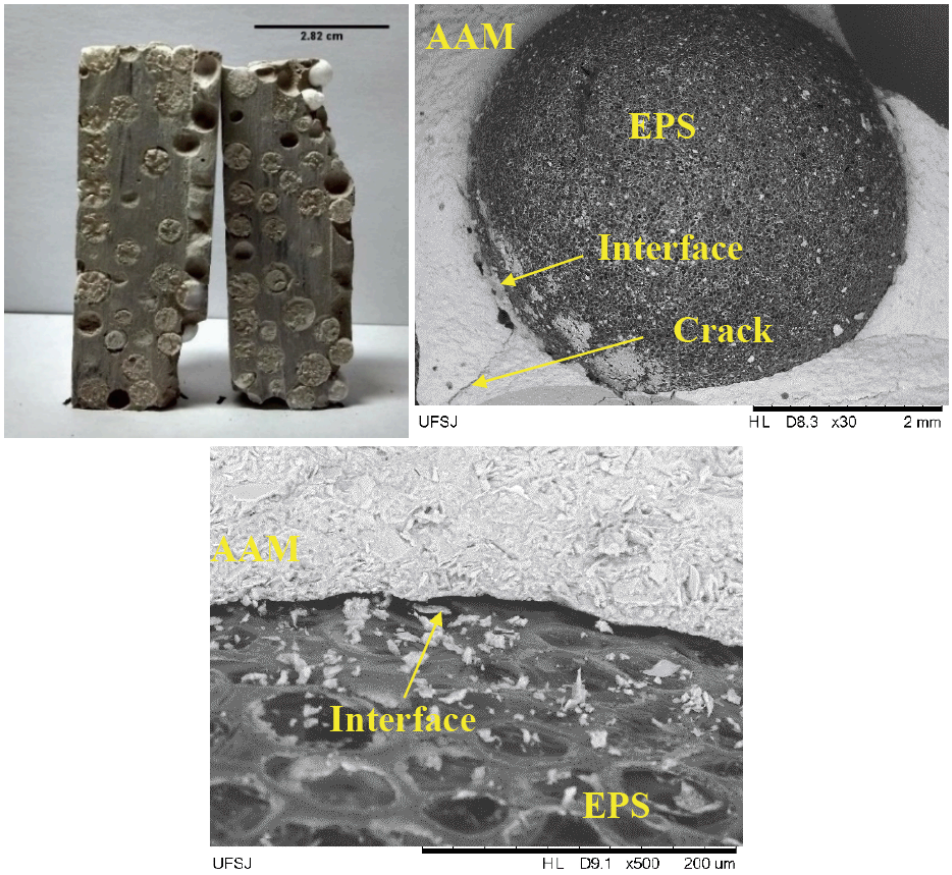

Figure 11: Longitudinal section and SEM images of composite 35C after 28 days.

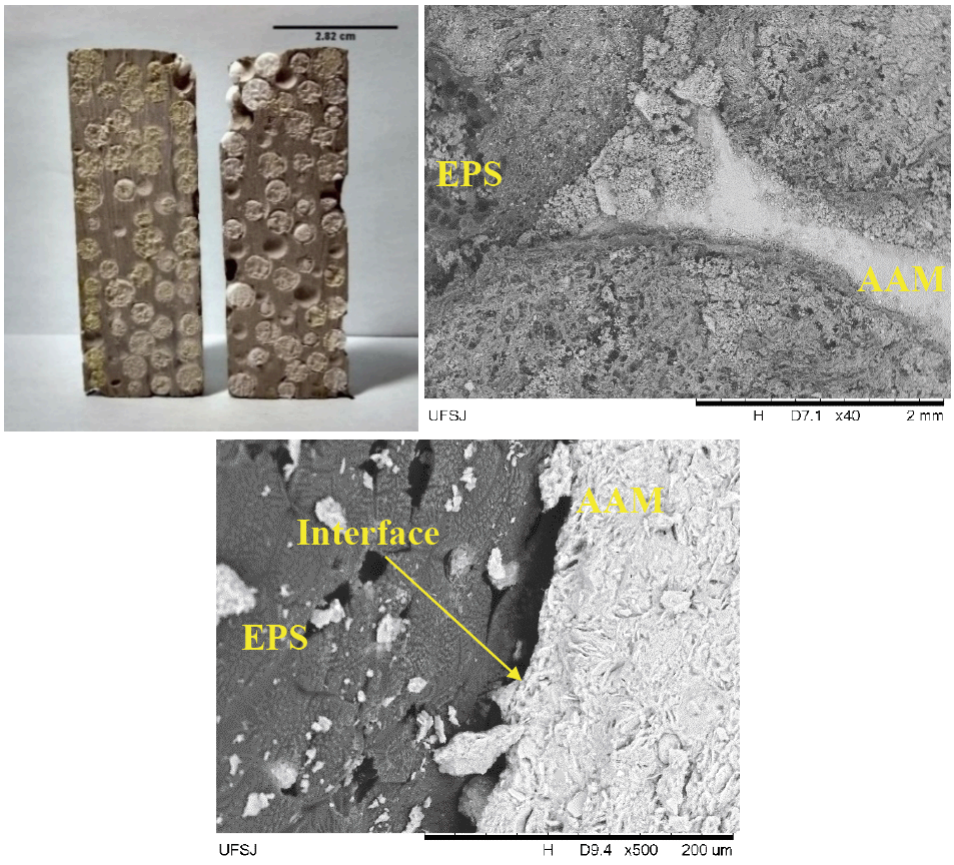

Figure 12: Longitudinal section and SEM images of composite 53C after 28 days.

interfacial gaps and local defects that act as preferential sites for crack initiation and propagation, explaining the greater reduction in compressive strength despite comparable composite densities.

3.5. Compressive Strength and Density–Strength Relationship

Figure **13** presents the 28-day compressive strength results. The reference alkali-activated matrix reached approximately 47.5 MPa. The addition of EPS reduced strength in all formulations, and the magnitude of this reduction depended on both particle content and size. For the smallest beads, compressive strength decreased to approximately 25 MPa at 18 vol.% EPS and 14 MPa at 53 vol.% EPS. When 6.00 mm beads were used, the corresponding strengths were about 12.2 and 1.5 MPa. Thus, increasing EPS content from 18 to 53 vol.% reduced the load-bearing fraction of the inorganic matrix, while increasing bead size intensified the detrimental effect of individual inclusions and their interfaces.

Only a limited number of studies have examined EPS in alkali-activated matrices. Colangelo *et al*. [25] reported compressive strengths of 3.4 and 1.8 MPa for metakaolin-based composites containing 65 and 72.5 vol.% recycled EPS particles, respectively. The tendencies observed here are also consistent with Portland-cement EPS concretes. Babu *et al*. [21], for example, showed that smaller EPS beads produced higher strength than larger beads at comparable mixture proportions. Together, these results indicate that the strength penalty associated with EPS is governed not only by its volume fraction, but also by particle geometry and the quality of the surrounding interfacial zone.

Although compressive strength generally decreased with decreasing density, the results demonstrate that density alone cannot fully explain the mechanical performance of the investigated composites. Formulations exhibiting comparable densities frequently developed markedly different compressive strengths, indicating that additional microstructural factors govern the load-bearing capacity of lightweight alkali-activated composites. The reduction in compressive strength is associated not only with the replacement of the load-bearing matrix by low-stiffness EPS particles, but also with changes in matrix continuity and interfacial characteristics. Increasing the EPS particle size enlarges the dimensions of the matrix-particle interfaces and reduces the continuity of the surrounding alkali-activated matrix. Consequently, larger interfacial defects become preferential sites for stress concentration and crack initiation during compressive loading. These observations are consistent with the SEM micrographs (Figure **7**-**12**), which reveal progressively larger interfacial discontinuities around the EPS particles, supporting the hypothesis that matrix continuity and interfacial integrity exert a decisive influence on the compressive behavior of the developed composites. The mechanical behavior discussed above is further elucidated by the SEM observations presented later in this section. As the EPS particle size increased, progressively larger interfacial discontinuities were observed between the polymeric inclusions and the alkali-activated matrix. These defects reduce the effective load-transfer area and promote stress concentration, explaining the lower

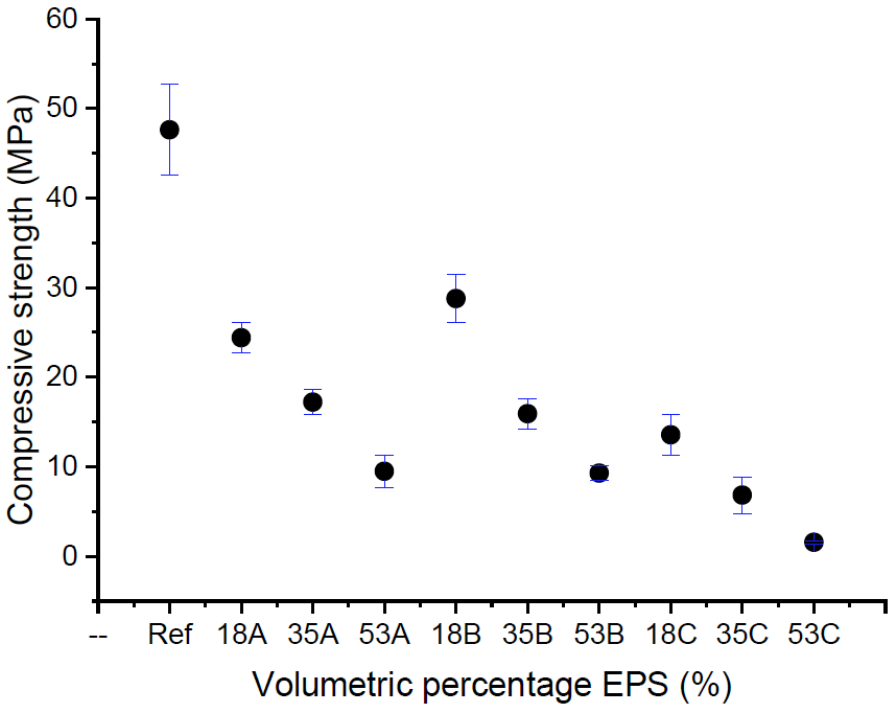

Figure 13: Compressive strength of the reference matrix and composites C1–C9 after 28 days.

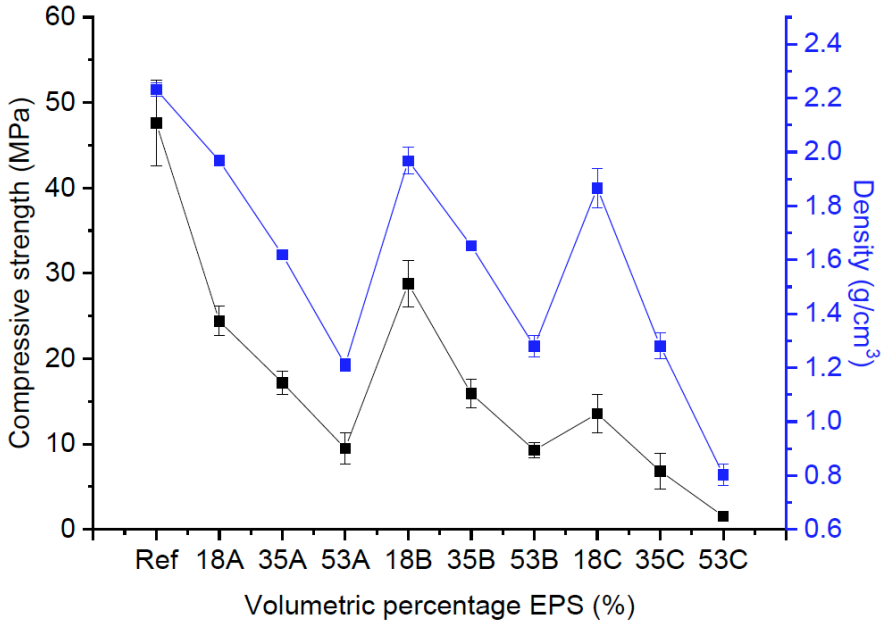

Figure 14: Relationship between compressive strength and density for the reference matrix and EPS-containing composites after 28 days.

compressive strengths obtained for formulations containing larger EPS particles.

The relationship between compressive strength and density is illustrated in Figure **14** and Table **6**. The two properties decrease concurrently because both are controlled by the replacement of the stiff, dense binder by low-density EPS. Nevertheless, density alone does not explain the full variation in strength. Composites with similar density but different bead sizes exhibited different compressive performance, confirming the additional influence of matrix continuity and interface quality. Fine EPS generated a larger number of smaller inclusions but preserved a more continuous load-bearing skeleton, whereas coarse beads introduced larger discontinuities and more severe local stress concentrations. From an application perspective, the most balanced formulations were those combining densities between approximately 0.8 and 1.2 g cm^{-3} with compressive strengths in the range of 15–25 MPa. These values support consideration of selected compositions for lightweight non-structural elements, although durability, thermal conductivity, fire behavior, and dimensional stability require further assessment.

The EPS-containing composites produced in the present study exhibited densities ranging from approximately 800 to 1980 kg/m³ and compressive strengths between 1.5 and 28.9 MPa. These ranges overlap those reported for several lightweight alkali-activated systems, while extending from ultra-light non-structural formulations to composites with moderate density and comparatively high mechanical performance. In particular, the formulations

Table 6: Density and Compressive Strength of the Lightweight Metakaolin-Based Alkali-Activated Composites Produced with Different EPS Volume Fractions and Particle Sizes

Formulation	EPS content (vol.%)	EPS size (mm)	Density (g/cm³)	Density (kg/m³)	Compressive strength (MPa)
Ref	0	—	2.23	2230	47.5
18A	18	0.85	1.97	1970	24.5
35A	35	0.85	1.63	1630	17.3
53A	53	0.85	1.22	1220	9.6
18B	18	2.16	1.98	1980	28.9
35B	35	2.16	1.66	1660	16.0
53B	53	2.16	1.29	1290	9.2
18C	18	6.00	1.88	1880	13.5
35C	35	6.00	1.29	1290	6.8
53C	53	6.00	0.80	800	1.5

containing 18 vol.% EPS achieved compressive strengths of up to approximately 28.9 MPa, exceeding the values commonly reported for highly porous or high-EPS alkali-activated composites. Conversely, the formulation containing 53 vol.% of the largest EPS beads reached a density of approximately 800 kg/m³ but retained only about 1.5 MPa, illustrating the mechanical limitation associated with combining high EPS content and large particle size.

The comparison among formulations with similar densities further demonstrates that density alone is insufficient to predict mechanical performance. For example, the 53A and 35C composites exhibited comparable densities of approximately 1220 and 1290 kg/m³, respectively, but compressive strengths of approximately 9.6 and 6.8 MPa. An even greater difference was observed between 18B and 18C: although their densities differed by only about 5%, the composite containing the largest EPS beads exhibited a compressive strength approximately 53% lower. These results indicate that matrix continuity, the dimensions of the matrix–EPS interfaces, and the associated stress concentration sites exert a decisive influence on compressive behavior.

Table **7** compares the density and compressive strength ranges obtained in the present study with representative lightweight alkali-activated composites containing EPS reported in the literature. Previous investigations consistently demonstrated that increasing the EPS content is an effective strategy for reducing composite density, although this improvement is generally accompanied by a significant reduction in compressive strength. Ultra-lightweight systems produced with high EPS contents or combined cellular structures typically achieve densities below 900 kg/m³ but exhibit compressive strengths below approximately 6 MPa. Conversely, formulations containing lower EPS contents or additional lightweight aggregates, such as expanded perlite, generally retain higher mechanical performance while exhibiting more moderate density reductions.

The present study covers a broad performance range, with densities varying from approximately 800 to 1980 kg/m³ and compressive strengths between 1.5 and 28.9 MPa, encompassing both ultra-lightweight and moderate-density composites. Compared with previous studies, the proposed experimental design provides a more systematic evaluation of the combined influence of EPS particle size and volume fraction on composite performance. Unlike most previous investigations, which primarily focused on EPS dosage, the present results demonstrate that density alone is insufficient to explain the mechanical behavior of lightweight alkali-activated composites. Formulations exhibiting similar densities frequently developed markedly different compressive strengths, indicating that matrix continuity, interfacial integrity, and EPS particle size also play fundamental roles in controlling mechanical performance. This behavior is particularly evident when comparing formulations with similar densities. For example, composites 53A and 35C exhibited densities of approximately 1220 and 1290 kg/m³, respectively, but compressive strengths of approximately 9.6 and 6.8 MPa. Likewise, composites 18B and 18C presented comparable densities (1980 and 1880 kg/m³), whereas the compressive strength decreased from approximately 28.9 to 13.5 MPa. These comparisons demonstrate that the reduction in mechanical performance cannot be attributed solely to density reduction. Instead, the larger EPS particles generate more pronounced interfacial discontinuities, reducing matrix continuity and promoting stress concentration sites that facilitate crack initiation and propagation during compressive loading. Unlike previous studies, the present work demonstrates that composites exhibiting comparable densities may develop substantially different compressive strengths depending on the EPS particle size. This finding highlights that optimizing lightweight alkali-activated

Table 7: Comparison between Lightweight Alkali-Activated Composites Containing EPS Reported in the Literature and the Present Study

Reference	Precursor	Lightweight system	EPS amount	Density (kg/m³)	Compressive strength (MPa)
Colangelo *et al*. [27]	Metakaolin	EPS beads	65–72.5 vol.%	516–827	1.8–6.0
Dueramae *et al*. [30]	Fly ash + calcium carbide residue	EPS beads	Binder/EPS = 1:2.50–1:3.00 (vol.)	750–900	1.5–3.0
Souza *et al*. [31]	Blast-furnace slag	EPS + cellular pores	Formulation-dependent	350–800	1.0–3.0
Kioupis *et al*. [32]	Fly ash	EPS + expanded perlite	Formulation-dependent	1000–1600	10.0–33.0
Kioupis *et al*. [33]	Recycled brick waste	Waste EPS	0.5–3.0 wt.%	1000–2100	6.5–22.8
Present study	Metakaolin	EPS beads	18–53 vol.%	800–1980	1.5–28.9

composites requires not only controlling the total EPS volume fraction but also carefully selecting the particle size distribution to preserve matrix continuity and improve stress transfer.

4. CONCLUSIONS

This study demonstrated that the performance of lightweight metakaolin-based alkali-activated composites is governed not only by the EPS volume fraction but also by the combined effects of particle size, matrix continuity, and matrix–particle interfacial characteristics. The main conclusions are as follows:

(1) Alkali activation successfully produced a predominantly disordered aluminosilicate binder, as evidenced by the displacement of the XRD amorphous halo and the shift of the principal Si–O–T FTIR band. EPS incorporation did not interfere with geopolymer formation, indicating that the polymeric inclusions acted primarily as lightweight aggregates rather than affecting the geopolymerization process.

(2) Increasing the EPS volume fraction progressively reduced composite density by replacing the dense aluminosilicate matrix with closed-cell polymeric particles. The lowest density (approximately 0.80 g cm^{-3}) was achieved using 53 vol.% of 6.00 mm EPS, demonstrating the effectiveness of EPS incorporation for producing ultra-lightweight alkali-activated composites.

(3) Water transport behavior could not be explained solely by apparent porosity. Although apparent porosity generally decreased with increasing EPS content, water absorption was increasingly governed by the morphology and connectivity of interfacial defects, particularly in composites containing coarse EPS particles. These results demonstrate that interfacial characteristics play a more significant role in fluid transport than the total accessible pore volume alone.

(4) Compressive strength was governed by the combined effects of density reduction and microstructural integrity. Although increasing EPS content reduced strength, composites with comparable densities exhibited markedly different compressive strengths depending on the EPS particle size. SEM observations revealed that coarse EPS particles generated wider interfacial discontinuities, reducing matrix continuity and the effective load-transfer area, thereby promoting stress concentration and crack propagation under compressive loading.

(5) The proposed approach enabled the production of lightweight alkali-activated composites with densities ranging from approximately 0.8 to 1.2 g cm^{-3} while maintaining compressive strengths up to 25 MPa, making them promising candidates for non-structural lightweight building applications. More importantly, the results demonstrate that optimizing lightweight alkali-activated composites requires balancing both EPS volume fraction and particle size to preserve matrix continuity and interfacial integrity, rather than considering density reduction alone. These findings provide practical design guidelines for the development of high-performance lightweight alkali-activated materials and contribute to a better understanding of the relationship between microstructure, interfacial characteristics, and mechanical performance.

ACKNOWLEDGMENT

The author gratefully acknowledge the financial support provided by the São Paulo Research Foundation (FAPESP) - FAPESP processes nº: 2024/02445-4 and 2025/11339-6.

AUTHOR'S CONTRIBUTION STATEMENT

N/A

CONFLICTS OF INTEREST STATEMENT

The author declare no conflict of interest.

REFERENCES

[1] Huiskes DMA, Keulen A, Yu QL, *et al*. Design and performance evaluation of ultra-lightweight geopolymer concrete. Mater Des 2016; 89: 516-26. https://doi.org/10.1016/j.matdes.2015.09.167

[2] Wianglor K, Sinthupinyo S, Piyaworapaiboon M, *et al*. Effect of alkali-activated metakaolin cement on compressive strength of mortars. Appl Clay Sci 2017; 141: 272-9. https://doi.org/10.1016/j.clay.2017.01.025

[3] Rovnaník P. Effect of curing temperature on the development of hard structure of metakaolin-based geopolymer. Constr Build Mater 2010; 24: 1176-83. https://doi.org/10.1016/j.conbuildmat.2009.12.023

[4] Mo BH, Zhu H, Cui XM, *et al*. Effect of curing temperature on geopolymerization of metakaolin-based geopolymers. Appl Clay Sci 2014; 99: 144-8. https://doi.org/10.1016/j.clay.2014.06.024

[5] Zhang M, Zhao M, Zhang G, *et al*. A multiscale investigation of reaction kinetics, phase formation, and mechanical properties of metakaolin geopolymers. Cem Concr Compos 2017; 78: 21-32. https://doi.org/10.1016/j.cemconcomp.2016.12.010

[6] Provis JL, Bernal SA. Geopolymers and related alkali-activated materials. Annu Rev Mater Res 2014; 44: 299-327. https://doi.org/10.1146/annurev-matsci-070813-113515

[7] Barroso MDB. Desenvolvimento de materiais geopoliméricos à base de metacaulim [doctoral thesis]. João Pessoa: Universidade Federal da Paraíba; 2009.

[8] Palomo A, Grutzeck MW, Blanco MT. Alkali-activated fly ashes: a cement for the future. Cem Concr Res 1999; 29: 1323-9. https://doi.org/10.1016/S0008-8846(98)00243-9

[9] Azevedo AGS. Assessment of Brazilian Type F fly ash: influence of chemical composition and particle size on alkali-activated materials properties. Powders 2026; 5: 2. https://doi.org/10.3390/powders5010002

[10] Kan A, Demirboğa R. A new technique of processing for waste-expanded polystyrene foams as aggregates. Cem Concr Compos 2009; 31: 489-95. https://doi.org/10.1016/j.cemconcomp.2009.05.002

[11] Ganesh Babu K, Saradhi Babu D. Behaviour of lightweight expanded polystyrene concrete containing silica fume. Cem Concr Res 2003; 33: 755-62. https://doi.org/10.1016/S0008-8846(02)01055-4

[12] Miled K, Le Roy R, Sab K, *et al*. Compressive behavior of an idealized EPS lightweight concrete: size effects and failure mode. Mech Mater 2004; 36: 1031-46. https://doi.org/10.1016/j.mechmat.2003.08.004

[13] Montgomery DC. Introduction to statistical quality control. 3rd ed. New York: John Wiley & Sons; 1997.

[14] Werkema MCC, Aguiar S. Planejamento e análise de experimentos: como identificar e avaliar as principais variáveis influentes em um processo. Belo Horizonte: Fundação Christiano Ottoni, Escola de Engenharia da UFMG; 1996.

[15] Domingos LFT, Azevedo AGS, Lombardi CT, *et al*. Corrosion resistance of fly ash-based geopolymer in hydrochloric and sulfuric acid solutions. Ceramica 2020; 66(380): 394-403. https://doi.org/10.1590/0366-69132020663802927

[16] Azevedo AGS, Strecker K, Araújo Jr AG, *et al*. Produção de geopolímeros à base de cinza volante usando soluções ativadoras com diferentes composições de Na_2O e Na_2SiO_3. Cerâmica 2017; 63(366): 143-51. https://doi.org/10.1590/0366-69132017633662078

[17] Azevedo AGS, Strecker K. Brazilian fly ash-based inorganic polymers production using different alkali activator solutions. Ceram Int 2017; 43(12): 9012-8. https://doi.org/10.1016/j.ceramint.2017.04.044

[18] Azevedo AGS, Strecker K, Barros LA, *et al*. Effect of curing temperature, activator solution composition and particle size in Brazilian fly ash-based geopolymer production. Mater Res 2019; 22(Suppl. 1): e20180686. https://doi.org/10.1590/1980-5373-mr-2018-0842

[19] Azevedo AGS, Strecker K, Lombardi CT. Produção de geopolímeros à base de metacaulim e cerâmica vermelha. Cerâmica 2018; 64: 388-96. https://doi.org/10.1590/0366-69132018643712420

[20] Li W, Lemougna PN, Wang K, *et al*. Effect of vacuum dehydration on gel structure and properties of metakaolin-based geopolymers. Ceram Int 2017; 43: 14340-6. https://doi.org/10.1016/j.ceramint.2017.07.190

[21] He P, Wang M, Fu S, *et al*. Effects of Si/Al ratio on the structure and properties of metakaolin based geopolymer Ceram Int 2016; 42: 14416-22. https://doi.org/10.1016/j.ceramint.2016.06.033

[22] Azevedo AGS, Strecker K. Brazilian fly ash-based inorganic polymers production using different alkali activator solutions. Ceram Int 2017; 43: 9012-8. https://doi.org/10.1016/j.ceramint.2017.04.044

[23] Ganesh Babu K, Saradhi Babu D. Performance of fly ash concretes containing lightweight EPS aggregates. Cem Concr Compos 2004; 26: 605-11. https://doi.org/10.1016/S0958-9465(03)00034-9

[24] Liu N, Chen B. Experimental study of the influence of EPS particle size on the mechanical properties of EPS lightweight concrete. Constr Build Mater 2014; 68: 227-32. https://doi.org/10.1016/j.conbuildmat.2014.06.062

[25] Kan A, Demirboğa R. Effect of cement and EPS beads ratios on compressive strength and density of lightweight concrete. Indian J Eng Mater Sci 2007; 14: 158-62.

[26] Azevedo AGS, Strecker K. Kaolin, fly-ash and ceramic waste based alkali-activated materials production by the "one-part" method. Constr Build Mater 2021; 269: 121306. https://doi.org/10.1016/j.conbuildmat.2020.121306

[27] Colangelo F, Roviello G, Ricciotti L, *et al*. Mechanical and thermal properties of lightweight geopolymer composites. Cem Concr Compos 2018; 86: 266-72. https://doi.org/10.1016/j.cemconcomp.2017.11.016

[28] Associação Brasileira de Normas Técnicas. ABNT NBR 5739: concreto — ensaio de compressão de corpos de prova cilíndricos. Rio de Janeiro: ABNT; 2007.

[29] International Organization for Standardization. ISO 10545-3: ceramic tiles — Part 3: determination of water absorption, apparent porosity, apparent relative density and bulk density. Geneva: ISO; 1997.

[30] Dueramae S, Sanboonsiri S, Suntadyon T, *et al*. Properties of lightweight alkali-activated controlled low-strength material using calcium carbide residue-fly ash mixture containing EPS beads. Constr Build Mater 2021; 297: 123769. https://doi.org/10.1016/j.conbuildmat.2021.123769

[31] Souza TB, Lima VME, Araújo FWC, *et al*. Alkali-activated slag cellular concrete containing expanded polystyrene (EPS): physical, mechanical and mineralogical properties. J Build Eng 2021; 44: 103387. https://doi.org/10.1016/j.jobe.2021.103387

[32] Kioupis D, Skaropoulou A, Tsivilis S, *et al*. Properties and durability performance of lightweight fly ash-based geopolymer composites incorporating expanded polystyrene and expanded perlite. Ceramics 2022; 5: 821-36. https://doi.org/10.3390/ceramics5040060

[33] Kioupis D, Skaropoulou A, Tsivilis S, *et al*. Development of lightweight geopolymer composites by combining various construction and demolition waste streams. Ceramics 2023; 6: 837-57. https://doi.org/10.3390/ceramics6020048

https://doi.org/10.31875/2410-4701.2026.13.05